




Kinetic concepts and local failure in the interfacial shear strength of epoxy-graphene nanocomposites

Spyros V. Kallivokas ^{*}, Aristotelis P. Sgouros ^{*}, and Doros N. Theodorou [†]

School of Chemical Engineering, National Technical University of Athens (NTUA), GR-15780 Athens, Greece



(Received 12 June 2020; accepted 2 September 2020; published 22 September 2020)

Interfacial shear strength (IFSS) is a key property in the design of composites and nanocomposites. Many simulation studies quantify the interfacial characteristics of sandwichlike specimens in terms of the IFSS and pullout force; a common feature of these studies is that they employ finite model systems and are therefore subject to strong finite size effects. We propose an alternative approach which is applicable to both aperiodic and periodic computational specimens. The interfaces are subjected to multiple shear deformation simulations over a wide range of temperatures (T) and shear stresses (σ_{zx}). From these simulations we collect the failure times (t_f); by analyzing them in the framework of an extended Boltzmann-Arrhenius-Zhurkov kinetic equation we derive the IFSS, the limiting stress for barrierless transitions, the activation energy, the activation volume for failure, the sliding velocities, and a local elastic shear modulus for the interface. We test our methodology on epoxy diglycidyl ether bisphenol F–diethyl toluene diamine interfaces in contact with (i) pristine graphene, (ii) graphene with single-atom vacancies, and (iii) graphene with hydroxyl-OH groups. Differences in the mechanism of interfacial failure among these three systems are discussed.

DOI: [10.1103/PhysRevE.102.030501](https://doi.org/10.1103/PhysRevE.102.030501)

Recent years have witnessed an emergent need for the development of advanced nanocomposite materials with tailored properties. Graphene has sparked the interest of researchers as a filler, since it exhibits record high elastic properties [1,2], thermal and electrical conductivity, and is impermeable to gases. A downside of pristine graphene is its limited ability to transfer stress to the matrix through the interface region; thus, the resulting nanocomposites cannot carry large loads due to premature interfacial failure [3]. To tackle this issue, several researchers have focused on functionalized or defected graphenic fillers [4–8]. The chemistry and morphology of the resulting interfaces lead to stronger matrix-filler interactions and thus enhance adhesive properties due to (i) strong covalent bonds between the filler and matrix [4,6–8], (ii) stronger electrostatic interactions due to charged groups, and (iii) mechanical interlocking that arises from the topography of both surfaces.

A popular approach for assessing the interfacial properties of nanocomposites is through molecular dynamics (MD) simulations of pullout experiments. These experiments are performed in sandwichlike geometries (i.e., planar geometries with alternating matrix-filler phases) that are aperiodic along the pullout direction. The filler and the epoxy matrix are displaced along opposite directions, leading to their eventual separation at long times. As these geometries are aperiodic, the intermolecular filler-matrix component of the potential energy, $E_{\text{matrix-filler}}$, tends to zero in the limit of large pull-out displacements. Hence, by monitoring and differentiating

$E_{\text{matrix-filler}}$ during the course of the pullout simulation one can obtain the force versus displacement curves and an estimate of the interfacial shear strength (IFSS) [3]. This approach has been employed in numerous studies in the past, such as in epoxy matrices with carbon nanotube fillers [4,6], and in epoxy-graphene nanocomposites [3,9–11].

Here we propose an alternative, kinetics-driven simulation approach for estimating the interfacial failure characteristics, which is applicable in sandwichlike geometries that are either aperiodic or fully periodic along the pullout direction. A detailed time-dependent study of local interfacial failure is conducted, introducing kinetic concepts. The filler and the matrix experience shear stresses σ_{zx} , with opposite magnitudes along the pullout direction, hence leading to noticeable displacement for large enough σ_{zx} . The simulations are carried out until simple displacement-dependent failure criteria are satisfied. For each combination of T and σ_{zx} we perform numerous simulations, and from each one we collect the failure times, if applicable. Afterwards, the set of failure times for each T and σ_{zx} is subjected to hazard analysis, from which we extract the characteristic failure time t_Z . Subsequently, T , σ_{zx} , and t_Z are input to a Boltzmann-Arrhenius-Zhurkov (BAZ) kinetic expression, leading to the macroscopic parameters for interfacial failure [12–14], i.e., the effective energy barrier (U), its interaction part (U_0), and the effective activation volume (γ). All these observables provide crucial information regarding stress transfer for any composite interface and can be used to parametrize predictive hierarchical modeling strategies for interfacial failure.

We apply our approach to epoxy matrix nanocomposites with various kinds of graphenic fillers. The epoxy is diglycidyl ether bisphenol F (DGEBF) (or EPON-862) and the cross-linking agent is diethyl toluene diamine (DETDA).

^{*}S.V.K. and A.P.S. contributed equally to this work.

[†]Corresponding author: doros@central.ntua.gr

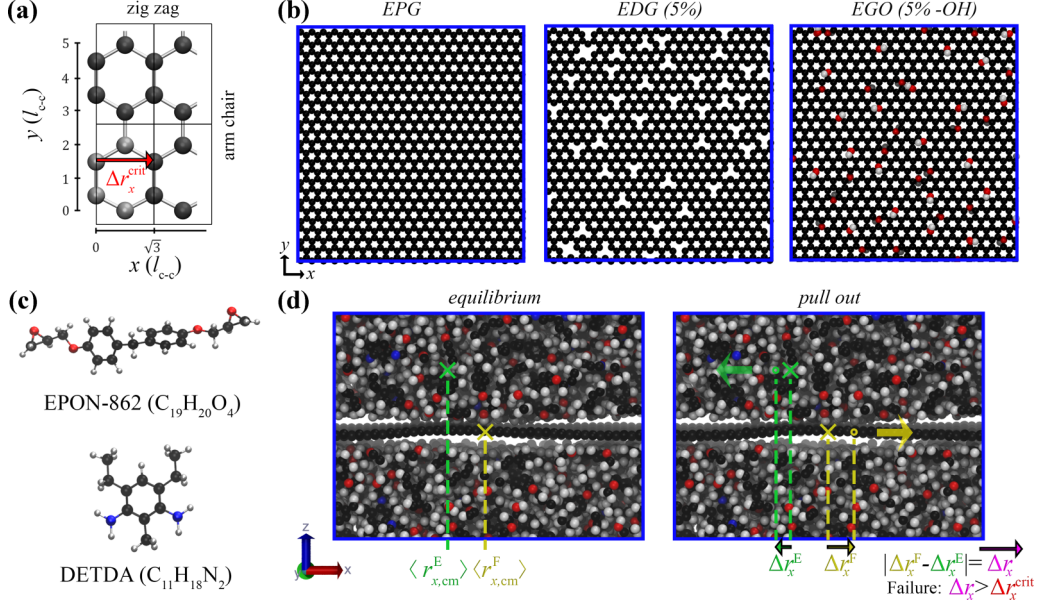


FIG. 1. (a) The four-atom orthogonal unit cell of graphene. (b) Atomistic representations [35] of (left) EPG, (middle) EDG, (right) EGO. (c) Representation of the EPON-862 epoxy resin and the DETDA cross linker. (d) Illustration of (left) the relaxation and (right) the pullout phases of the experiment. The green (yellow) \times marker depicts the equilibrium-averaged center of mass of the epoxy (filler).

Three kinds of fillers are examined: (i) pristine graphene (EPG), (ii) graphene with vacancies (EDG), and (iii) graphene oxide (EGO); see Fig. 1(b). Even though we have not considered chemical bonding between the filler and the matrix phases, our simulation approach could be extended to cases where chemical bonds are present across the interface [15].

The configurations [16] were subjected to pullout experiments as shown in Fig. 1(d) by applying on both the graphite and polymer phases equal and opposite total external forces in the x direction. From the external force F_x applied we estimate the interfacial shear stress as $\sigma_{zx} = F_x / \langle A_{xy} \rangle$ with $\langle A_{xy} \rangle = 2l_x l_y$ being the total contact area between the filler and the epoxy. An interface is considered fractured when the relative filler-matrix displacement, $\Delta r_x = |(r_{x,cm}^F - \langle r_{x,cm}^F \rangle) - (r_{x,cm}^E - \langle r_{x,cm}^E \rangle)| = |\Delta r_x^F - \Delta r_x^E|$, exceeds a critical value Δr_x^{crit} , which was set to the lattice constant of graphene. More details regarding the model systems and the simulation parameters can be found in Ref. [17] and in Supplemental Material Sec. S1 [18].

A local shear modulus was extracted from the slope of the stress versus displacement ($\sigma_{zx} / \langle \Delta r_x \rangle$) curve in the low stress regime. The local shear modulus for the interface was derived as $G^{if} = \sigma_{zx} / \varepsilon_{zx}^{if}$, with $\varepsilon_{zx}^{if} = \langle \Delta r_x \rangle / \Delta z_{E-G}$ defining a local interfacial shear strain; $\Delta z_{E-G} = 0.37$ nm was taken as the closest distance between the graphite peak and an epoxy atom peak in the density distribution along the z direction. The

G^{if} versus T plots are shown in Fig. S2 of the Supplemental Material [18]. The slope, dG^{if}/dT , and the extrapolation $G_{T=0}^{if}$ of G^{if} in the limit $T = 0$ K are shown in Table I. As expected, the lowest $G_{T=0}^{if}$ is observed in EPG; in EDG $G_{T=0}^{if}$ is slightly higher; while in EGO it is higher by about an order of magnitude at 369 MPa, indicating best adhesion. For an order of magnitude comparison, the shear modulus of EPON-862 resin is ~ 1 GPa according to experiments [36] and simulations [17], while the Winkler modulus of poly(methyl methacrylate) with embedded bilayer graphenes multiplied by $\Delta z_{E-G} = 0.37$ nm is ~ 370 MPa [37].

Figure 2 presents the mean times to local fracture t_f for EPG, EDG, and EGO as functions of σ_{zx} for $T = 20$ –300 K. σ_{zx} corresponds to IFSS which has been shown to be both temperature and strain-rate dependent for $T < T_g$, albeit there have been conflicting trends in the literature depending on the conditions of the experiments [38,39]. For $\sigma_{zx} < \sigma_{lim}$, t_f decreases exponentially with σ_{zx} ; the drop becomes less steep with increasing temperature, suggesting an $\sim \exp[\gamma \sigma_{zx} / (k_B T)]$ dependence [12]. For $\sigma_{zx} \sim \sigma_{lim}$, the plot in Fig. 2 features a “knee,” after which t_f becomes independent of temperature and all curves collapse to a power law, $t_f \sim \sigma_{zx}^{-0.5}$, in the limit of large σ_{zx} , indicating accelerating motion. The aforementioned suggest the manifestation of two distinct failure mechanisms depending on the magnitude of the imposed stress, as explained below.

TABLE I. Parameters of EPG, EDG, and EGO.

System	U_0 (kcal/mol)	γ (nm ³)	σ_{lim} (MPa)	τ_{lim} (ps)	dG^{if}/dT (MPa/K)	$G_{T=0}^{if}$ (MPa)
EPG	3.9	5.4	5.0	5.5	-0.231	64.0
EDG	9.1	9.2	6.9	4.8	-0.175	71.1
EGO	11.1	0.7	114.9	1.2	-0.560	369.0

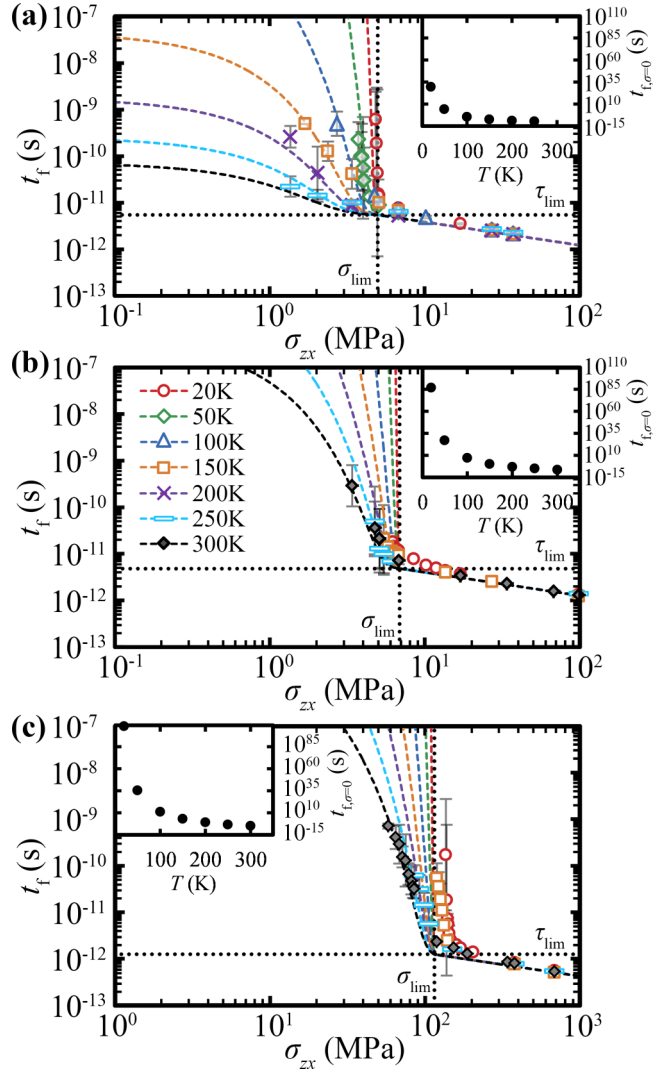


FIG. 2. Mean failure times for (a) EPG, (b) EDG, and (c) EGO. The dashed lines are fits to the extended BAZ equation [Eq. (3)]. The vertical (horizontal) dotted line delimits σ_{lim} (τ_{lim}). The insets show the extrapolated fracture times for $\sigma_{zx} = 0$ vs temperature.

A popular model for describing fracture behavior is embodied in the Boltzmann-Arrhenius-Zhurkov (BAZ) equation [12]. Zhurkov extended the Arrhenius [40,41] expression for the temperature dependence of the rate of thermally activated infrequent events, which in turn invokes Boltzmann statistics. The BAZ equation considers that the free energy barrier that has to be overcome for an infrequent transition to occur is modified by the imposition of an external force; the work associated with that force adds a bias to the energy hypersurface of the system. The fracture rate is thus determined by both temperature and mechanical stress:

$$t_Z = \tau_0 \exp\left(\frac{U_0 - \gamma\sigma_{zx}}{k_B T}\right). \quad (1)$$

U_0 is the magnitude of the energy barrier in the absence of stress, γ is an activation volume which indicates the volume of the region responsible for the cohesion of the interface, and τ_0 is usually set to the natural oscillation frequency of atoms which is in the order of 10^{-13} s. σ_{lim} corresponds to the

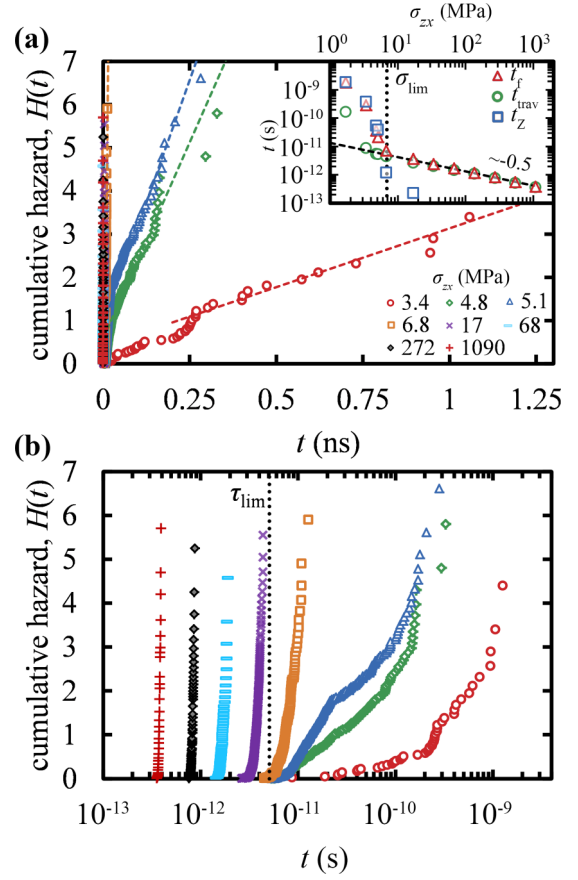


FIG. 3. The cumulative hazard function $H(t)$ based on the failure times of EDG at $T = 300$ K in (a) linear and (b) semilog plots. The dashed lines in (a) represent linear fits and the dotted line in (b) corresponds to $\tau_{\text{lim}} = 4.8$ ps. The inset shows t_f , t_{trav} , and t_Z ; the vertical dotted line illustrates $\sigma_{\text{lim}} = 6.9$ MPa, and the dashed line corresponds to the second branch of Eq. (3) ($\sigma_{zx} \geq \sigma_{\text{lim}}$).

stress value for which the exponent becomes zero; thus, $\sigma_{\text{lim}} = U_0/\gamma$. Consequently, for $\sigma_{zx} = \sigma_{\text{lim}}$, the failure time becomes $t_Z = \tau_0$ [12]. However, our simulations suggest a somewhat different picture: at the limiting stress σ_{lim} we observe, t_Z collapse to a limiting value (τ_{lim} , denoted by the horizontal dotted line in Fig. 2), which is orders of magnitude longer than 10^{-13} s. In our simulations, τ_{lim} does not correspond to an oscillation frequency; instead, it is a basin traversal time $t_Z = \tau_{\text{lim}}$ for $\sigma_{zx} = \sigma_{\text{lim}}$ that exhibits a dependency on the system's constitution.

To discern the contributing mechanisms we performed hazard analysis on the failure time distributions $\rho(t)$. The cumulative hazard function $H(t)$ is computed with respect to the list of sorted failure times $\mathbf{t}_{T,\sigma_{zx}} = (t_1, t_2, \dots, t_N)_{T,\sigma_{zx}}$ using the estimate $H(t_i) = \sum_{j=1}^i 1/(N-j+1)$ [42]. The slope of $H(t)$ equals the hazard function, $h(t) = dH(t)/dt$ which corresponds to the probability density for failure at time t ; therefore, high (low) slope indicates high (low) failure rates. Figure 3 depicts the cumulative hazard function $H(t)$ for EDG at $T = 300$ K. From the semilog plot in Fig. 3(b) one can discern two distinct regimes:

(i) There is an initial time period (t_{trav}) before failure and this is reflected in the value $H(t) = 0$ at short times.

During this time, the filler experiences shearing forces and is displaced relative to the polymer, the configuration of the whole system moving towards the edge of its local energy basin.

(ii) After time t_{trav} the filler may slip, its displacement exceeding Δr_x^{crit} , and this is reflected in an increase of $H(t)$ due to the accumulation of failure events. At short times, $H(t)$ exhibits nonlinearities, while for longer times $H(t)$ increases linearly with time, suggesting a Poisson-like rate process, shifted in time by t_{trav} . Poisson processes have the property that the slope of $H(t)$ is constant and equals the failure rate which is the inverse of the mean residence time in the basin t_Z . More information about fitting $H(t)$ for estimating t_Z can be found in Supplemental Material Sec. S4 [18].

Based on the above kinetic analysis the mean failure times can be approximated as

$$t_f \sim t_Z + t_{\text{trav}} \simeq \begin{cases} t_Z, & \sigma_{zx} \ll \sigma_{\text{lim}} \\ t_{\text{trav}}, & \sigma_{zx} \gg \sigma_{\text{lim}} \end{cases}, \quad (2)$$

while any discrepancies can be traced to the nonlinearities of $H(t)$ for moderate stresses. It is instructive to examine the limiting cases for low and high shear stresses: (i) for low stresses ($\sigma_{zx} \ll \sigma_{\text{lim}}$), t_{trav} becomes negligibly small in comparison to the failure time ($t_{\text{trav}} \ll t_f$). Therefore, t_f is practically equal to t_Z , and they can be described very well by the macroscopic BAZ equation [Eq. (1)]; e.g., compare triangles, t_f , with squares, t_Z , in the inset to Fig. 3(a). (ii) For high stresses ($\sigma_{zx} \gg \sigma_{\text{lim}}$), t_{trav} follows the power law with respect to stress presented in the inset to Fig. 3(a) and becomes the dominant term in Eq. (2), since the transitions become barrierless and $t_Z \rightarrow 0$; e.g., compare triangles, t_f , with circles, t_{trav} , in the inset to Fig. 3(a).

We formulated an extension to the BAZ model which is as follows:

$$t_f = \begin{cases} \tau_0 e^{(U_0 - \gamma \sigma_{zx}) / (k_B T)} + \tau_{\text{lim}}, & \sigma_{zx} \leq \sigma_{\text{lim}} \\ \sqrt{2 \rho_A \Delta r_x^{\text{crit}} / \sigma_{zx}}, & \sigma_{zx} \geq \sigma_{\text{lim}} \end{cases}, \quad (3)$$

where U_0 , γ , and τ_0 are Zhurkov's macroscopic material constants, and $\rho_A = \tilde{m} / A_{xy}$ is the areal reduced mass density with $\tilde{m} = m_{\text{filler}} m_{\text{epoxy}} / (m_{\text{filler}} + m_{\text{epoxy}})$ being the reduced mass of the two body system; note that $\lim_{m_{\text{epoxy}} \rightarrow \infty} \tilde{m} = m_{\text{filler}}$. Essentially, the first branch of Eq. (3) extends Zhurkov's equation to incorporate a characteristic traversal time period. It models failure as a delayed Poisson process in which the material is unable to fail at very small times, and only after time τ_{lim} does it have a chance to fail. τ_{lim} is commensurate to the time required for the material to "wake up from inertia." τ_0 is associated with the oscillation frequency of the interface and thus relates to the failure rate dictating the pure Poisson process. A similar picture could be manifested in experiments but these traversal times are way too small to be observed. By setting $\tau_{\text{lim}} = 0$ we obtain the original BAZ equation [Eq. (1)]. The second branch of Eq. (3) for $\sigma_{zx} \geq \sigma_{\text{lim}}$ considers that the filler is decoupled from the matrix and is accelerating under constant applied force.

Equation (3) requires three parameters (τ_0 , U_0 , γ), which are determined as discussed in Secs. S5 and S6 of the Supplemental Material [18]. From the master curves shown in Fig. 4 one can derive γ as the slope, and U_0 as the intercept

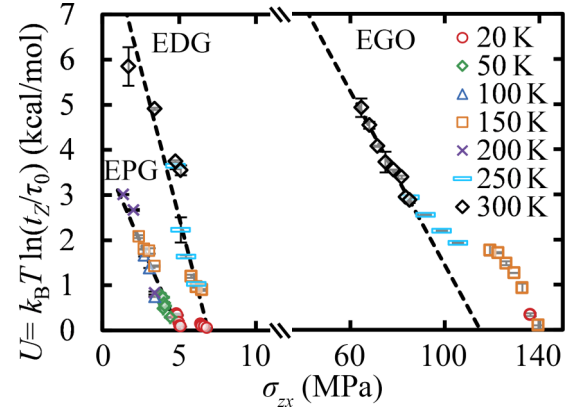


FIG. 4. Effective energy barrier vs shear stress for: (left) EPG, (middle) EDG, and (right) EGO.

of a linear fit. Note that EGO presents a complicated behavior at low temperatures, thus the slope for this case was taken from the higher temperatures, since these are more relevant experimentally. The $U(\sigma_{zx})$ dependence in EGO exhibits a parallel shift in the region around 250 K. We attribute this effect to a change in the segmental mobility of the polymer, which affects the mechanism of reinforcement of the interface by $-\text{OH}$ groups; for more details please see Supplemental Material Sec. S7 [18].

The fitted parameters are displayed in Table I. EPG features the lowest energy barrier and this conforms with the short failure times [3]. The highest U_0 is that of EGO and this is attributed to the strong interactions of $-\text{OH}$ groups with epoxy plus the rougher geometry produced by sp^3 carbons, which promotes mechanical interlocking with the polymer at the atomistic level. The estimated effective barriers are about an order of magnitude lower than experimental ones on relevant systems [3,11,12,43]. This is not unexpected, given that our simulations correspond to local interfacial failure at the atomistic level, while experiments reflect macroscopic fracture, which results from a cascade of such atomistic failure events over a not necessarily perfectly flat interface. Moreover, the γ for EPG and EDG is larger than that for EGO by about an order of magnitude. This is because in EPG and EDG the process of overcoming the energy barrier under externally imposed shear involves interactions across an extended—more or less molecularly smooth—surface (the holes in EPG do not perturb this smoothness), while in EGO the process of overcoming the barriers is localized to the vicinity of the $-\text{OH}$ functional groups. The predicted γ 's conform with experimental estimates for relevant systems, e.g., for DGEBA-based epoxy with p -aramid fibers, $\gamma \sim 3.1 \text{ nm}^3$ [38].

Figure 2 illustrates evaluations of Eq. (3), which provide a good description of simulation findings. The insets in Fig. 2 depict t_f in the absence of shearing forces ($\sigma_{zx} = 0$); the graphenic fillers are practically static for temperatures lower than 100 K, while at room temperature the probability for spontaneous transitions becomes considerable. For all stresses, $t_f^{\text{EPG}} < t_f^{\text{EDG}} \ll t_f^{\text{EGO}}$. Literature findings from previous MD studies are compared against the failure times (t_f) from our work in Table S1, Sec. S8, of the Supplemental Material [18]. Our IFSS values for EPG are similar to (larger

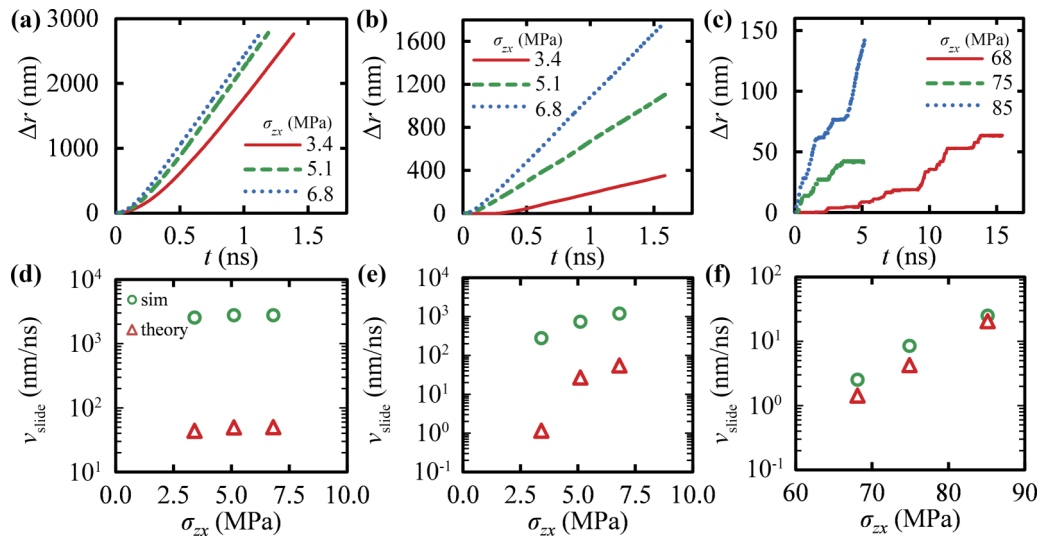


FIG. 5. The postfailure displacement of (a) EPG, (b) EDG, and (c) EGO at 300 K as a function of time. The circles in (d)–(f) depict the sliding velocities based on the slopes of the time vs displacement plots in (a)–(c), respectively; the triangles depict analytic evaluations based in Eq. (4).

than) IFSS from periodic [44] (aperiodic [11]) systems along the pullout direction.

With t_f known, one can attempt a prediction of the postfailure sliding velocities for $\sigma_{zx} < \sigma_{lim}$, based on the following expression:

$$v_{slide}^{theory}(t) = \Delta r_x^{crit} / t_f, \sigma_{zx} < \sigma_{lim}. \quad (4)$$

For $\sigma_{zx} < \sigma_{lim}$, t_f corresponds to the time needed for the filler to become displaced by Δr_x^{crit} . Unless the potential energy hypersurface has been perturbed significantly during the sliding of the filler, the sliding velocity is expected to be constant. In order to assess the validity of these predictions we performed additional simulations for all systems at 300 K with

the fillers being displaced indefinitely after the initial failure. In Fig. 5, the simulated sliding velocity (v_{slide}^{sim}) of both EPG and EDP plateaus to a value that is ~ 2 orders of magnitude higher than v_{slide}^{theory} from Eq. (4). Agreement is good for EGO, suggesting that the postfailure dynamics can be described as a sequence of “stick-slip” events (see the visualization in Sec. S9 of the Supplemental Material [18]).

S.V.K. gratefully acknowledges financial support through a Doctoral fellowship of the E. Eugenides Foundation, Athens, Greece. A.P.S. is grateful for financial support by SOLVAY, Paris, France, through the project “Multiscale Modeling for the Design of Antifouling Copolymers.”

-
- [1] K. S. Novoselov, A. K. Geim, S. V. Morozov, D. Jiang, Y. Zhang, S. V. Dubonos, I. V. Grigorieva, and A. A. Firsov, *Science* **306**, 666 (2004).
- [2] A. K. Geim and K. S. Novoselov, *Nat. Mater.* **6**, 183 (2007).
- [3] L. S. Melro, R. Pyrz, and L. R. Jensen, *IOP Conf. Ser. Mater. Sci. Eng.* **139**, 012036 (2016).
- [4] K. Guru, S. B. Mishra, and K. K. Shukla, *Appl. Surf. Sci.* **349**, 59 (2015).
- [5] C. Li, A. R. Browning, S. Christensen, and A. Strachan, *Compos. Part A Appl. Sci. Manuf.* **43**, 1293 (2012).
- [6] S. J. V. Frankland, A. Caglar, D. W. Brenner, and M. Griebel, *J. Phys. Chem. B* **106**, 3046 (2002).
- [7] Q. Zheng, Y. Geng, S. Wang, Z. Li, and J. K. Kim, *Carbon N. Y.* **48**, 4315 (2010).
- [8] Z. Qin and M. Buehler, *Mol. Simul.* **38**, 695 (2012).
- [9] M. Li, H. Zhou, Y. Zhang, Y. Liao, and H. Zhou, *RSC Adv.* **7**, 46101 (2017).
- [10] M. C. Wang, Z. B. Lai, D. Galpaya, C. Yan, N. Hu, and L. M. Zhou, *J. Appl. Phys.* **115**, 123520 (2014).
- [11] F. Liu, N. Hu, M. Han, S. Atobe, H. Ning, Y. Liu, and L. Wu, *Mol. Simul.* **42**, 1165 (2016).
- [12] S. N. Zhurkov, *Int. J. Fract. Mech.* **1**, 311 (1965).
- [13] E. Suhir and S. M. Kang, *Mod. Phys. Lett. B* **27**, 1330009 (2013).
- [14] E. Suhir, *Int. J. Aeronaut. Sci. Aerosp. Res.* **6**, 185 (2019).
- [15] S. D. Anogiannakis, C. Tzoumanekas, V. Georgilas, and D. N. Theodorou, in *Proceedings of the 16th International Conference on Deformation, Yield, and Fracture of Polymers (DYFP2015)* (Rolduc, Kerkrade, The Netherlands, 2015), pp. 2–6.
- [16] MAPS @ version 4.2 Scienomics Paris (2020).
- [17] S. V. Kallivokas, A. P. Sgouros, and D. N. Theodorou, *Soft Matter* **15**, 721 (2019).
- [18] See Supplemental Material at <http://link.aps.org/supplemental/10.1103/PhysRevE.102.030501>, which includes Refs. [19–34], for technical details, derivations, and numerical simulations.
- [19] S. L. Mayo, B. D. Olafson, and W. A. Goddard III, *J. Phys. Chem.* **94**, 8897 (1990).
- [20] D. N. Theodorou and U. W. Suter, *Macromolecules* **18**, 1467 (1985).
- [21] C. Li and A. Strachan, *Polymer* **51**, 6058 (2010).
- [22] S. Plimpton, *J. Comput. Phys.* **117**, 1 (1995).

- [23] R. W. Hockney and J. W. Eastwood, *Computer Simulation Using Particles* (Taylor & Francis, New York, 1988).
- [24] S. Nose, *J. Chem. Phys.* **81**, 511 (1993).
- [25] W. G. Hoover, A. J. C. Ladd, and B. Moran, *Phys. Rev. Lett.* **48**, 1818 (1982).
- [26] W. C. Swope, H. C. Andersen, P. H. Berens, and K. R. Wilson, *J. Chem. Phys.* **76**, 637 (1982).
- [27] R. Z. Wan, S. Y. Li, and H. P. Fang, *Chin. Phys. Lett.* **27**, 084702 (2010).
- [28] J. Wong-ekkabut and M. Karttunen, *Biochim. Biophys. Acta - Biomembr.* **1858**, 2529 (2016).
- [29] M. Vögele and G. Hummer, *J. Phys. Chem. B* **120**, 8722 (2016).
- [30] A. P. Sgouros, G. G. Vogiatzis, G. Kritikos, A. Boziki, A. Nikolakopoulou, D. Liveris, and D. N. Theodorou, *Macromolecules* **50**, 8827 (2017).
- [31] S. Li, X. Liu, C. Fang, N. Liu, and D. Liu, *RSC Adv.* **8**, 20505 (2018).
- [32] B. Qi, Z. Yuan, S. Lu, K. Liu, S. Li, L. Yang, and J. Yu, *Fibers Polym.* **15**, 326 (2014).
- [33] D. Yoon, Y. Son, and H. Cheong, *Nano Lett.* **11**, 3227 (2011).
- [34] Y. Li, Y. Liu, X. Peng, C. Yan, S. Liu, and N. Hu, *Comput. Mater. Sci.* **50**, 1854 (2011).
- [35] W. Humphrey, A. Dalke, and K. Schulten, *J. Mol. Graph.* **14**, 33 (1996).
- [36] J. L. Tack, Masters thesis, Texas A&M University, College Station, Texas, 2006.
- [37] C. Androulidakis, E. N. Koukaras, M. G. Pastore Carbone, M. Hadjinicolaou, and C. Galiotis, *Nanoscale* **9**, 18180 (2017).
- [38] A. Straub, M. Slivka, and P. Schwartz, *Compos. Sci. Technol.* **57**, 991 (1997).
- [39] A. N. Netravali, R. B. Henstenburg, S. L. Phoenix, and P. Schwartz, *Polym. Compos.* **10**, 226 (1989).
- [40] S. Arrhenius, *Z. Phys. Chem.* **4U**, 96 (1889).
- [41] S. Arrhenius, *Z. Phys. Chem.* **4U**, 226 (1889).
- [42] A. P. Sgouros, G. G. Vogiatzis, G. Megariotis, C. Tzoumanekas, and D. N. Theodorou, *Macromolecules* **52**, 7503 (2019).
- [43] Y. J. Shur, B. Rånby, K. Chung, and S. Kim, *Polym. Eng. Sci.* **18**, 812 (1978).
- [44] Z. Q. Zhang, D. K. Ward, Y. Xue, H. W. Zhang, and M. F. Horstemeyer, *ISRN Mater. Sci.* **2011**, 145042 (2011).